

Comparatively high in-field critical current in type-II superconductors from heterogeneous columnar pins: a molecular dynamics study

J. P. Rodriguez, E. J. Oswald

Department of Physics and Astronomy, California State University at Los Angeles, Los Angeles, CA 90032

Abstract

Theoretical work predicts that the strong dependence of T_c on pure shear strain within the a - b plane of optimally doped $\text{YBa}_2\text{Cu}_3\text{O}_{7-\delta}$ results in heterogeneous columnar pins of vortex lines about dislocation lines and about nano-columns inclusions aligned in parallel to the c axis. The critical current of a rigid vortex lattice driven by the Lorentz force in the presence of such clusters of pin/antipin lines is computed using two-dimensional (2D) collective pinning theory and by numerical simulation of the corresponding 2D vortex dynamics. Both theory and computer calculation find that the antipin component of the heterogeneous columnar pins contributes substantially to the net in-field critical current.

Key words:

in-field critical current, nanorod inclusions, strain field

1. Introduction

Optimally doped films of the high- T_c superconductor $\text{YBa}_2\text{Cu}_3\text{O}_{7-\delta}$ (YBCO) grown by pulsed laser deposition (PLD) show high critical currents that reach a substantial fraction of the theoretical maximum depairing current in applied magnetic field oriented in parallel to the c axis[1]. Evidence exists that this is primarily due to edge dislocations that thread the film along the c axis in PLD-YBCO[2]. The critical current of YBCO films in c -axis aligned applied magnetic field can also be enhanced substantially by the introduction of BaZrO_3 (BZO) or of BaSnO_3 (BSO) material that naturally form nanorods along the c axis during the film growth process[3][4][5]. Such increases

in the in-field performance of the critical current in YBCO films by columnar microstructures are very important to the development of second-generation high- T_c superconducting wire technology. Achieving a fundamental understanding of how they occur is therefore desirable.

In this paper, we shall compute the in-field critical due to natural or to artificial columnar microstructures in YBCO thin films by employing two-dimensional (2D) collective pinning theory[6][7] and by performing direct computer simulations of the corresponding 2D vortex dynamics[8][9][10][11][12][13][14]. Pinning of vortex lines will be assumed to be due to variations in T_c about columnar defects that in turn are a result of the strain field about them[15]. Heterogeneous columnar defects are thereby predicted that are composed of component lines of pins and of antipins of equal strength[16][17]. These form a dipolar “clover-leaf” pattern in the case of an edge dislocation line defect (see fig. 1), while they form a quadropolar pattern in the case of a nano-column inclusion (see fig. 2). Both 2D collective pinning theory[6][7] and direct computer simulation of 2D vortex dynamics obtain the following central result: that the critical current due to an arrangement of weak heterogeneous columnar pins is equal to that expected from an arrangement of conventional columnar pins[18] obtained by unbinding the component pin/antipin lines from the heterogeneous cluster, and by then converting the isolated antipin lines that result into pin lines of equal strength. Figure 3 depicts the two pinning landscapes in question. The antipin components of heterogeneous columnar defects therefore increase the critical current by a factor of two compared to the contribution due to the true pin components alone in the collective pinning regime.

2. Strain/pinning landscape about material line defects in YBCO

It is well known that the critical temperature in optimally doped YBCO couples most strongly to pure shear strain in the a - b plane[15]. In particular, the variation in the critical temperature depends linearly on the symmetric strain tensor $\epsilon_{\alpha,\beta} = (\partial_\alpha u_\beta + \partial_\beta u_\alpha)/2$ following

$$\delta T_c(\mathbf{r}) = \sum_{\alpha} \sum_{\beta} (\partial T_c / \partial \epsilon_{\alpha,\beta}) \epsilon_{\alpha,\beta}(\mathbf{r}) \quad (1)$$

with strain derivatives $\partial T_c / \partial \epsilon_{aa} = 230$ K and $\partial T_c / \partial \epsilon_{bb} = -220$ K. Below, we shall show how the shear strain about a line of edge dislocations or about a

nano-column inclusion in a YBCO thin film combined with this experimental fact results in a heterogeneous columnar pinning line for a vortex line in the mixed state.

Consider a line of edge dislocations that threads a YBCO film in parallel to the c axis. Gurevich and Pashitskii calculated the variation in the critical temperature expected from a linear dependence on strain (1) and obtained the result[16]

$$\delta T_c(\mathbf{r}) = \left(T_{\parallel} \frac{1-2\sigma}{1-\sigma} \pm T_{\perp} \frac{\cos^2\phi}{1-\sigma} \right) \frac{b \sin\phi}{2\pi r}, \quad (2)$$

with constants[15]

$$T_{\parallel} = -\frac{1}{2} \left(\frac{\partial T_c}{\partial \epsilon_{aa}} + \frac{\partial T_c}{\partial \epsilon_{bb}} \right) = -5 \text{ K}, \quad (3)$$

$$T_{\perp} = \frac{\partial T_c}{\partial \epsilon_{bb}} - \frac{\partial T_c}{\partial \epsilon_{aa}} = -450 \text{ K}. \quad (4)$$

Above, σ denotes the Poisson ratio and b denotes the magnitude of the Burgers vector. It can be aligned along either the a (+) or the b (-) axes. We now note that the contribution of the vortex core to the vortex line tension is approximated by the fundamental energy scale per unit length $\varepsilon_0 = (\Phi_0/4\pi\lambda_L)^2$, where λ_L denotes the London penetration depth, and where Φ_0 denotes the flux quantum in a type-II superconductor. The potential-energy landscape experienced by a vortex line then has a contribution $\delta\varepsilon_1(\mathbf{r}) = (\partial\varepsilon_0/\partial T_c) \cdot \delta T_c(\mathbf{r})$ due to the variation in the critical temperature about the dislocation line (2). It is dominated by the shear component (T_{\perp}) in the case of optimally doped YBCO, which is shown in fig. 1. The potential energy landscape is essentially dipolar in such case, with two anti-pinning lobes (+) and two pinning lobes (-).

An analogous heterogeneous pinning potential for a vortex line about a nano-column inclusion has been obtained more recently by one of the authors in collaboration with Barnes and Varanasi[17]. The lattice mismatch between the inclusion and the YBCO matrix results in pure shear strain about the inclusion. These authors then ultimately find a variation of the critical temperature in the YBCO matrix about the nano-column given by

$$\delta T_c(\mathbf{r}) = T_{\perp} \frac{\Delta r}{r_{\text{out}}} \frac{c_{\parallel}^{(\text{in})}}{c_{\parallel}^{(\text{in})} + c_{\perp}^{(\text{out})}} \left(\frac{r_{\text{out}}}{r} \right)^2 \cos 2\phi. \quad (5)$$

Here $\Delta r = r_{\text{in}} - r_{\text{out}}$ is the mismatch between the radius of the inclusion, r_{in} , and the radius of the corresponding void in the YBCO matrix, r_{out} , while $c_{\parallel}^{(\text{in},\text{out})}$ and $c_{\perp}^{(\text{in},\text{out})}$ are the 2D compression and shear moduli, respectively. The potential-energy landscape experienced by a vortex line again then has a contribution $\delta\varepsilon_1(\mathbf{r}) = (\partial\varepsilon_0/\partial T_c) \cdot \delta T_c(\mathbf{r})$ due to such a variation in the critical temperature about the nano-column inclusion, but with d-wave symmetry. Figure 2 depicts the constant-energy contours. Notice that the potential energy is characterized by diametrically opposite lobes of pins and of antipin oriented with respect to each other by 90 degrees.

Last, the force $\mathbf{f}_1(\mathbf{r}) = -\nabla \varepsilon_1(\mathbf{r})$ that a vortex core experiences due to changes in T_c about both a line of edge dislocations (2) and about a nanocolumn inclusion (5) is long-range. Suppose now that a random field of parallel lines of heterogeneous pins thread a YBCO film along c axis at transverse locations $\{\mathbf{R}_i\}$. Statistical cancellations in the net force experienced by a vortex core, $\mathbf{f}(\mathbf{r}) = \sum_i \mathbf{f}_1(\mathbf{r} - \mathbf{R}_i)$, cut off the long-range force. The effective finite range r_p of each heterogeneous pin is determined by matching the fluctuation in the net force over the system with the long-range force due to a single material line defect: $\overline{f^2} = |\mathbf{f}_1(r_p)|^2$. It is given by the expression $r_p = (2/\pi n_\phi)^{1/6} r_{\text{out}}^{2/3}$ in the case of strain-induced pinning of vortex lines about nano-column inclusions[17], where n_ϕ denotes their density.

3. Collective pinning of Abrikosov vortex lattice by heterogeneous columnar pins

Above, we have shown how the strain field about edge dislocations and nano-column inclusions that thread a YBCO film along the c axis result in heterogeneous pinning lines for vortex lines that are present in the mixed phase. As shown by figs. (1) and (2), the heterogeneous columnar pins are clusters with equal numbers of pins and antipin, each of equal strength. [See also Eqs. (2) and (5).] Consider now a YBCO film threaded by a field of such heterogeneous pinning lines in applied magnetic field aligned along the c axis as well. Next, suppose that a rigid vortex lattice appears as a result. Among the fraction of vortex lines that experience forces from the heterogeneous columnar pins, half will lie in valleys of the vortex-core potential while the other half will lie on the hills of the vortex-core potential. Because the magnitude of the force experienced by the vortex lines that lie in the valleys and on the hills of the vortex-core potential are equal, the critical current should be the same as that due to a field of columnar pins which results

from (i) unbinding the cluster of pins and antipins from the heterogeneous pins, and (ii) converting each of the antipins that are now isolated into pins of equal strength and range. Figure 3 depicts the two columnar pinning arrangements in question for the case of nano-column inclusions. Below, we shall see that this prediction is indeed borne out by 2D collective pinning theory.

Previous work by one of the authors and Maley[7] implies that many heterogeneous columnar defects collectively pin a rigid Abrikosov vortex lattice. Theoretical arguments and numerical Monte Carlo simulations indicate, in particular, that a hexatic Bose glass state can exist at low temperature in such a case[19][20]. Here the vortex lattice is threaded by isolated lines of edge dislocations parallel to the lines of relatively weak pins/anti-pins. (See fig. 4.) The critical current j_c is then limited by plastic creep of the vortex lattice associated with glide by such edge dislocations[7]. Application of 2D collective pinning theory[6] yields a transverse Larkin scale R_c that is set by the density of Larkin domains

$$R_c^{-2} \sim n_p (f_p / c_{66} b_\Delta)^2. \quad (6)$$

Here n_p denotes the density of vortex lines pinned by the material line defects and f_p denotes the maximum force per unit length at a pin/antipin that makes up the heterogeneous material line defect. Also, c_{66} denotes the shear modulus of the vortex lattice, while b_Δ is the magnitude of Burgers vectors that glide. It can be shown that R_c is of order the separation between isolated lines of dislocations in the hexatic Bose glass[21]. A statistical summation of the pinning forces inside of a corresponding Larkin volume, in which the vortex lattice is perfectly rigid, then yields a net pinning force density

$$j_c B / c \sim n_p f_p^2 / c_{66} b_\Delta. \quad (7)$$

The above is valid if many vortex lines experience pinning forces inside of a Larkin volume: $n_p R_c^2 \gg 1$. Last, study of equations (2) and (5) shows that the potential energy about a heterogeneous pinning line experienced by a vortex line has zero angle average. This implies that the occupation of a heterogeneous pin by a vortex line is purely random. The density of vortex lines that they collectively pin is then equal to $n_p = (\sigma_p n_B) n_\phi$, where n_ϕ denotes the density of heterogeneous columnar defects, where $\sigma_p = \pi(r_p^2 - r_{\text{out}}^2)$ is the effective crosssectional area of a heterogeneous pinning/antipinning line, and where n_B denotes the density of vortex lines. Observe now that both f_p

and the product $n_\phi\sigma_p$ remain constant after unbinding the pins and anti-pins that make up heterogeneous columnar defects, and after then converting the isolated antipins that result into isolated true pins! We conclude that 2D collective pinning theory[7][6] implies that the critical current due to comparable arrangements of conventional columnar pins and of heterogeneous columnar pins like those shown in fig. 3 are the same.

4. Computer simulation of 2D vortex dynamics

We shall now compute the in-field critical current due to columnar pins instead by simulating over-damped vortex dynamics with the Langevin equation. Our aim is to once again compare the critical-state performance of type-II superconductors threaded by conventional columnar pins[18] with that of type-II superconductors threaded by heterogeneous (d-wave) pinning lines that can result from the strain field about nano-column inclusions in YBCO[17]. The Abrikosov vortex lattice in a field of parallel columnar pins is in a Bose glass state characterized by an infinite macroscopic tilt modulus[22]. The longitudinal Larkin scale L_c is then infinite[19], which means that vortex lines may be considered as rigid rods at long longitudinal length scales. In a film geometry that is perpendicular the applied magnetic field, their dynamics can therefore be described by the over-damped 2D Langevin equations for the transverse motion of a given rigid vortex line at location \mathbf{r} [8][9][10][11][12][13][14]:

$$\eta\dot{\mathbf{r}} = \sum_{\mathbf{r}'} \mathbf{F}_{vv} + \mathbf{F}_{vp} + \mathbf{F}_{\text{Lorentz}} + \mathbf{F}_{\text{Brown}}(t). \quad (8)$$

It is governed by the Bardeen-Stephen viscosity η for a vortex line. Each rigid vortex line experiences forces $\mathbf{F}_{vv} = -\nabla U_{vv}$ and $\mathbf{F}_{vp} = -\nabla U_{vp}$ due to interactions with other vortices at locations \mathbf{r}' and due to the field of material line defects, respectively. The former is taken to be long range:

$$U_{vv}(\mathbf{r}, \mathbf{r}') = \frac{4\pi\epsilon_0 d}{N_x N_y} \sum_{\mathbf{q} \neq 0} \frac{\exp[\mathbf{q} \cdot (\mathbf{r} - \mathbf{r}')] }{4 - 2\cos(q_x a) - 2\cos(q_y a)}. \quad (9)$$

Note that periodic boundary conditions are imposed over a rectangle of dimensions $N_x a \times N_y a$. The lattice constant a of the grid is understood to be of order the diameter of a vortex core. Above, d denotes the thickness of the film. Values for both potential energies U_{vv} and U_{vp} that span a $N_x \times N_y$

grid are stored in look-up tables. The corresponding forces \mathbf{F}_{vv} and \mathbf{F}_{vp} are computed from these potentials by taking finite differences over the grid. They are also stored in look-up tables. Last, a force at an arbitrary location is determined by linear interpolation from those determined off the grid.

In the special case of a featureless (S-wave) line pin that lies at a grid point (ma, na) , the above linear interpolation scheme yields a pinning force of the form

$$\begin{aligned} f_x^{(p)}(x, y) &= f_{1D}^{(p)}(x - ma) \cdot g(y - na), \\ f_y^{(p)}(x, y) &= g(x - ma) \cdot f_{1D}^{(p)}(y - na), \end{aligned}$$

where $f_{1D}^{(p)}$ is the pinning force along a principal axis of the grid that contains the pinning center. Both it and its corresponding 1D potential energy $u_{1D}^{(p)}$ are shown in fig. 5. The scale $f_0^{(p)}$ that appears there denotes the magnitude of the maximum pinning force, which is related to the depth $u_0^{(p)}$ of the line pin potential by $f_0^{(p)} = u_0^{(p)}/a$. The transverse interpolation of forces is set by the function g , which is also shown in fig. 5. It is given explicitly by $g(y) = 1 - |y/a|$ if $|y| < a$, and by $g(y) = 0$ otherwise. Notice now that $\partial_x f_y^{(p)} \neq \partial_y f_x^{(p)}$, which means that the above force field for a line pin is not conservative. On the other hand, leaving the 1D function g free while imposing a conservative force implies that it must be given by $g(y) = -u_{1D}^{(p)}(y)/f_0^{(p)}a$ instead. As shown by fig. 5, both functions have qualitatively similar shapes. They both also have the same area, $\int_{-\infty}^{+\infty} dy g(y) = a$. We believe, therefore, that the model for a linear pin displayed by the equations above is qualitatively correct.

The rigid vortex lines also experience a uniform Lorentz force $\mathbf{F}_{\text{Lorentz}}$ that push them across the width of the wire, in addition to a random Brownian force $\mathbf{F}_{\text{Brown}}(t)$ that brings the vortex lattice into thermal equilibrium. We numerically evolved the above Langevin equation (8) in order to describe the over-damped dynamics of 896 rigid vortex lines. The second-order Runge-Kutta method was employed. Values for the interaction forces and for the pinning forces to be stored in look-up tables were determined by taking finite differences over a 224×224 square grid that spans the system, and which has a lattice constant a that is understood to be of order the superconducting coherence length. The computer simulations were conducted in two stages. We first annealed the vortex lattice down to low temperature in the presence of a landscape of weak columnar pins. Figure 3 depicts the two pinning (anti-pinning) landscapes that were studied. All (component) line pins had equal

strengths, each with a maximum pinning/antipinning energy $u_0^{(p)} = f_0^{(p)}a$ equal to 1% of the dominant interaction scale $2\varepsilon_0d$. The initial temperature was taken to be very many times the Halperin-Nelson-Young melting temperature of the 2D vortex lattice, $T_m^{(2D)}$, and it was successively halved until a very small fraction of $T_m^{(2D)}$ was reached. Two million time steps were taken at each temperature, with a time interval Δt equal to a few percent of the natural time scale $\eta a_v^2/4\pi\varepsilon_0d$ that is set by the dominant interaction energy among vortex lines, Eq. (9). Here $a_v = (\Phi_0/B)^{1/2}$ is the average separation between vortex lines. The annealed vortex lattice was found to be in a hexatic vortex glass state characterized by long-range orientational order and unbound dislocations[19][20][23]. Only a fraction of the vortices in the lattice experience pinning forces. In the second stage, we drove the annealed vortex lattice at zero temperature with a uniform Lorentz force in the presence of the same landscape of columnar pins. The driving force increased in 300 steps from zero to about twice the critical force (current). Each step of constant Lorentz force lasted 200,000 time iterations, Δt , and the Lorentz force was increased at each step by a part in 100,000 of the interaction scale $2\varepsilon_0d/a_v$.

Figure 6 shows the current-voltage properties that result from driving the vortex lattice at zero-temperature through the pinning landscapes that are shown in fig. 3. The landscape in the left panel is the field of conventional (S-wave) columnar pins that is shown in the left panel of fig. 3. All of the pins in this case are featureless and of equal strength, with a number that matches the number of vortex lines (896). As depicted by fig. 5, each pin lies at a grid point and inherits the minimum range of the grid. Notice the critical current that separates a pinned vortex lattice at low currents from a vortex lattice that experiences flux creep and flux flow at high currents. It is interesting to note that although the vortex lattice was threaded by isolated dislocation defects throughout the simulation, these became well separated precisely at the critical state. (See figs. 4 and 6.) The dislocation defects then gradually began to pair up and annihilate with increasing driving force in the flux-creep/flux-flow regime. The right panel of fig. 6 displays the current-voltage property for a driven vortex lattice that experiences the arrangement of quadrupolar columnar pins that is shown in the right panel of fig. 3. The latter aims to model the strain-induced pinning potential shown in fig. 2 that is predicted to exist about nano-column inclusions in YBCO films[17]. This pinning landscape contains half the number (2×224) of true line pins, by

comparison with the previous case, with an equal number (2×224) of antipin lines. Each component line of pins/antipins has the same range and strength as in the previous case, on the other hand. Figure 6 indicates that the critical current in the present case of heterogeneous columnar pins is comparable to that obtained in the previous case of featureless columnar pins, which had *twice* the number of true pins! This result is nevertheless anticipated by 2D collective pinning theory, Eq. (7). It is due to the fact that the pin and the antipin components of the heterogeneous pinning line contribute equally to the critical current of a rigid vortex lattice. Last, two well-spaced dislocation defects with equal and opposite Burgers vectors threaded the vortex lattice throughout the second simulation.

5. Conclusions

In summary, strain about columnar microstructure in YBCO films generates heterogeneous pin/antipin lines that can multiply the critical current expected from the true pin line components alone by a factor of two. This result is obtained for weak correlated pinning inside of the collective pinning regime, however. It is unlikely to persist in the limit of strong correlated heterogeneous pins, where all vortex lines that experience pinning forces then lie along a true pin component of the composite line defect. Antipin line components of the heterogeneous pin have no effect on the critical current in that limit. A key assumption of the collective pinning analysis is that the critical state be found in a hexatic Bose glass state characterized by isolated dislocation defects that thread the vortex lattice[7]. Figure 4 demonstrates that this assumption is indeed confirmed by the molecular dynamics simulations that we conducted across the critical state for 896 rigid vortex lines. Previous 2D simulations find evidence for the break-up of the vortex lattice into grains at much higher numbers of rigid vortex lines when the latter experience short-range interactions[13][14]. Thermodynamic Monte Carlo simulations on over 2000 vortices that experience the same long-range logarithmic interaction studied here, Eq. (9), find evidence for an equilibrium hexatic vortex glass phase[19], on the other hand. It therefore remains to be seen if the hexatic glass phase obtained in the present molecular-dynamics simulations persists in the thermodynamic limit.

JPR thanks Paul Barnes and Hsin-Ju Wu for discussions. This work was supported in part by the US Air Force Office of Scientific Research under grant no. FA9550-06-1-0479.

References

- [1] S. R. Foltyn, L. Civale, J. L. MacManus-Driscoll, Q. X. Jia, B. Maiorov, H. Wang and M. Maley, *Nature Materials* **6**, 631 (2007).
- [2] F.C. Klaassen, G. Doornbos, J.M. Huijbregtse, R.C.F. van der Geest, B. Dam and R. Griessen, *Phys. Rev. B* **64**, 184523 (2001).
- [3] J.L. MacManus-Driscoll, S.R. Foltyn, Q.X. Jia, H. Wang, A. Serquis, L. Civale, B. Maiorov, M.E. Hawley, M.P. Maley and D.E. Peterson, *Nature Materials* **3**, 439 (2004).
- [4] A. Goyal, S. Kang, K.J. Leonard, P.M. Martin, A.A. Gapud, M. Varela, M. Paranthaman, A.O. Ijaduola, E.D. Specht, J.R. Thompson, D.K. Christen, S.J. Pennycook and F.A List, *Supercond. Sci. Technol.* **18**, 1533 (2005).
- [5] C.V. Varanasi, J. Burke, L. Brunke, H. Wang, M. Sumption and P.N. Barnes, *J. Appl. Phys.* **102**, 063909 (2007).
- [6] P.H. Kes and C.C Tsuei, *Phys. Rev. B* **28**, 5126 (1983).
- [7] J.P. Rodriguez and M.P. Maley, *Phys. Rev. B* **73**, 094502 (2006).
- [8] H.J. Jensen, Y. Brechet and A. Brass, *J. Low Temp. Phys.* **74**, 293 (1989).
- [9] A.E. Koshelev and V.M. Vinokur, *Phys. Rev. Lett.* **73**, 3580 (1994).
- [10] N. Gronbech-Jensen, A.R. Bishop and D. Dominguez, *Phys. Rev. Lett.* **76**, 2985 (1996).
- [11] M.C. Faleski, M.C. Marchetti and A.A. Middleton, *Phys. Rev. B* **54**, 12427 (1996).
- [12] S. Ryu, M. Hellerqvist, S. Doniach, A. Kapitulnik and D. Stroud, *Phys. Rev. Lett.* **77**, 5114 (1996).
- [13] M. Chandran, R.T. Scalettar, G. Zimanyi, *Phys. Rev. B* **69**, 024526 (2004).
- [14] M. Chandran, *Int. J. Mod. Phys. B* **19** (12), 1995 (2005).

- [15] U. Welp, M. Grimsditch, S. Fleshler, W. Nessler, J. Downey, G.W. Crabtree, and J. Guimpel, Phys. Rev. Lett. **69**, 2130 (1992).
- [16] A. Gurevich and E.A. Pashitskii, Phys. Rev. B **56**, 6213 (1997).
- [17] J.P. Rodriguez, P.N. Barnes and C.V. Varanasi, Phys. Rev. B **78**, 052505 (2008).
- [18] L. Civale, A.D. Marwick, T.K. Worthington, M.A. Kirk, J.R. Thompson, L. Krusin-Elbaum, Y. Sun, J.R. Clem, and F. Holtzberg, Phys. Rev. Lett. **67**, 648 (1991).
- [19] J.P. Rodriguez, Phys. Rev. B **76**, 224502 (2007).
- [20] Y. Nonomura and X. Hu, Europhys. Lett. **65**, 533 (2004).
- [21] S.J. Mullock and J.E. Evetts, J. Appl. Phys. **57**, 2588 (1985).
- [22] D.R. Nelson and V.M. Vinokur, Phys. Rev. B **48**, 13060 (1993).
- [23] E. M. Chudnovsky, Phys. Rev. B **43**, 7831 (1991).

HETEROGENEOUS PINNING ABOUT EDGE DISLOCATION

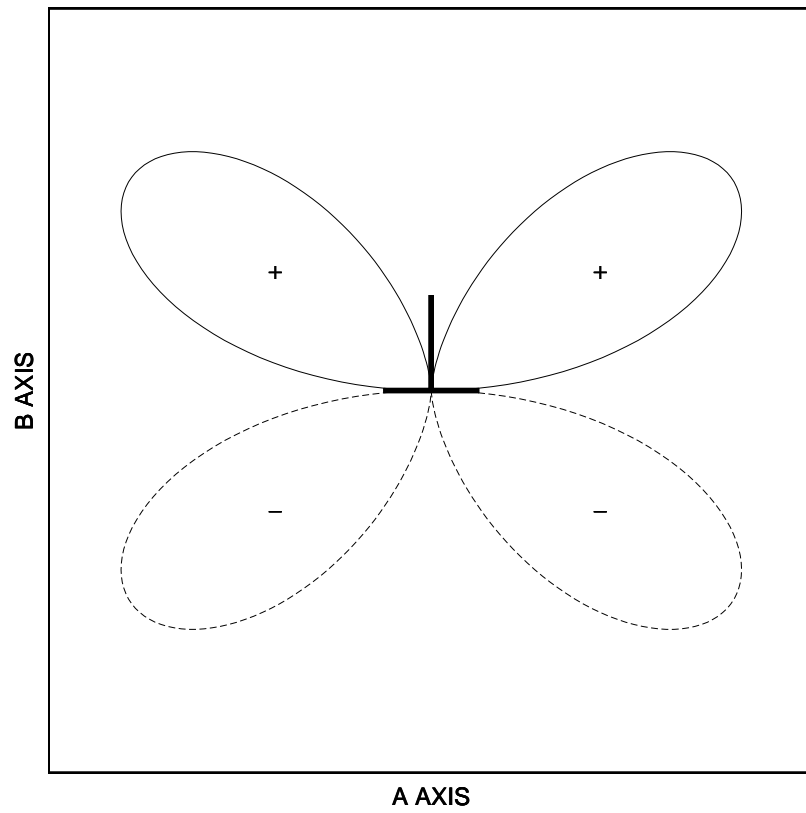


Figure 1: Shown is the contour of a potential-energy landscape for a vortex core about an edge dislocation aligned parallel to the c axes of optimally doped YBCO at two fixed energies $\pm\varepsilon_1$.

HETEROGENEOUS PINNING ABOUT NANO-COLUMN INCLUSION

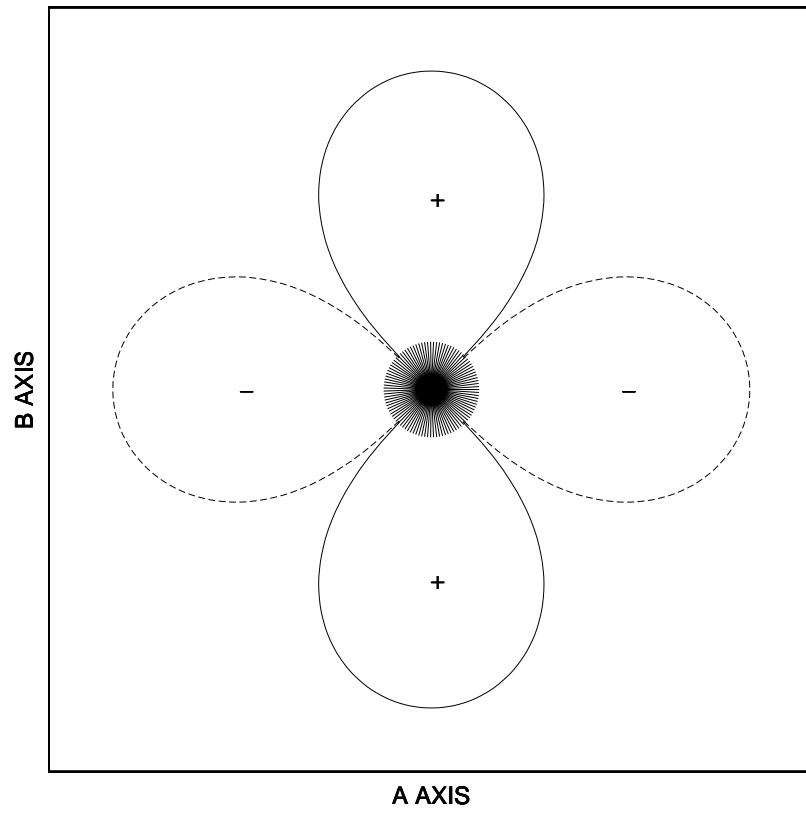


Figure 2: Contours for the potential energy of a vortex core about a nano-column inclusion in YBCO are depicted for two fixed energies $\pm\varepsilon_1$.

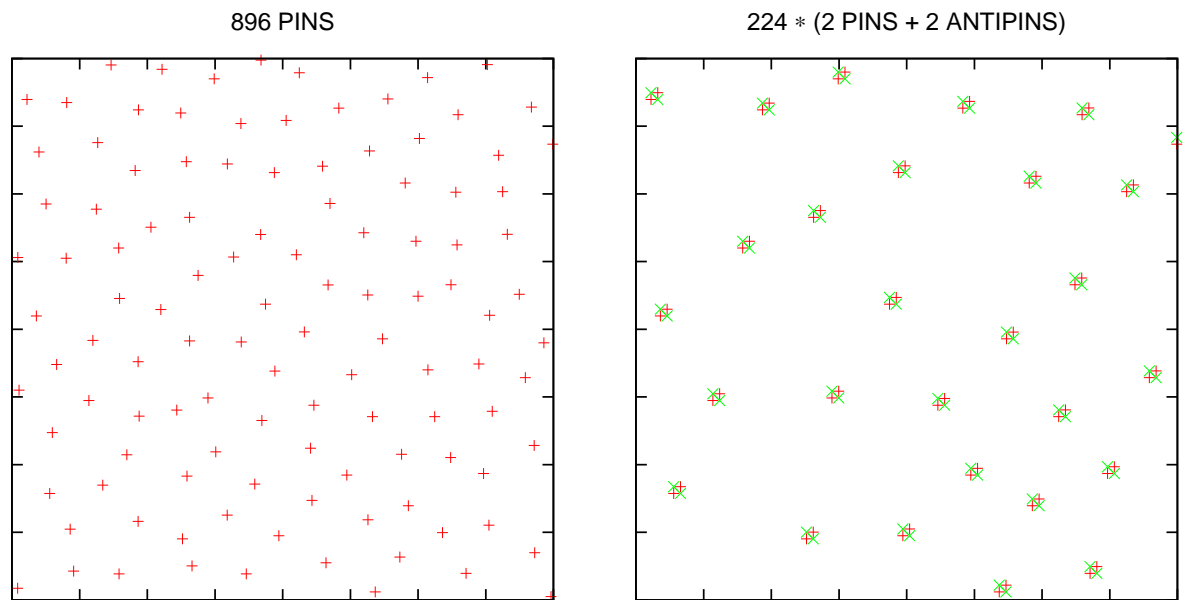


Figure 3: Shown above are windows of equal area into an arrangement of conventional columnar pins (+) and into an arrangement of quadrupolar columnar pins (+ \times , \times +) that can result from shear strain about nano-column inclusions.

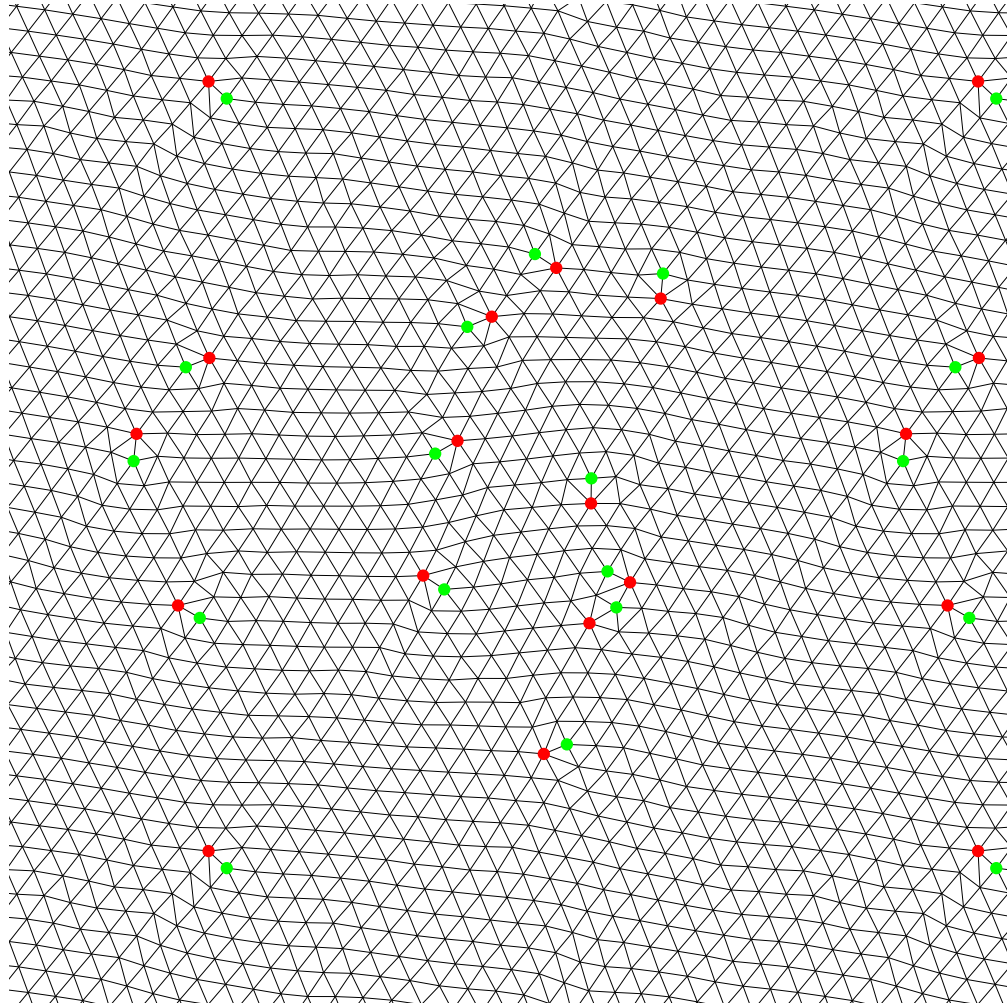


Figure 4: Shown is the critical-state configuration of 896 rigid vortex lines in the presence of an equal number of conventional columnar pins. (See the left panel in fig. 6.) Pairs of red and green dots mark dislocation defects in the triangular vortex lattice.

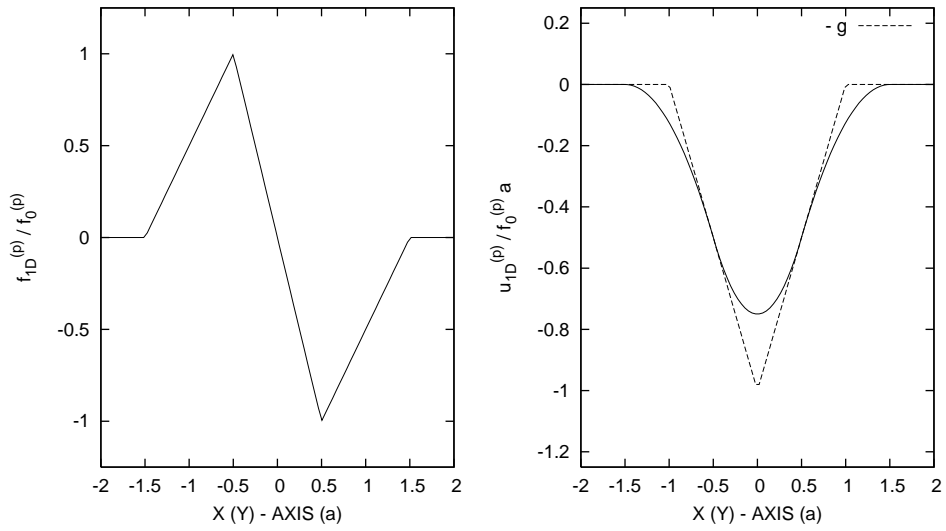


Figure 5: The solid lines above depict the pinning force and the corresponding potential energy along principal axes ($x = 0$ or $y = 0$) due to a featureless point defect that lies on the square lattice grid at point $(0, 0)$. The force at a general point (x, y) is determined by linear interpolation over the grid.

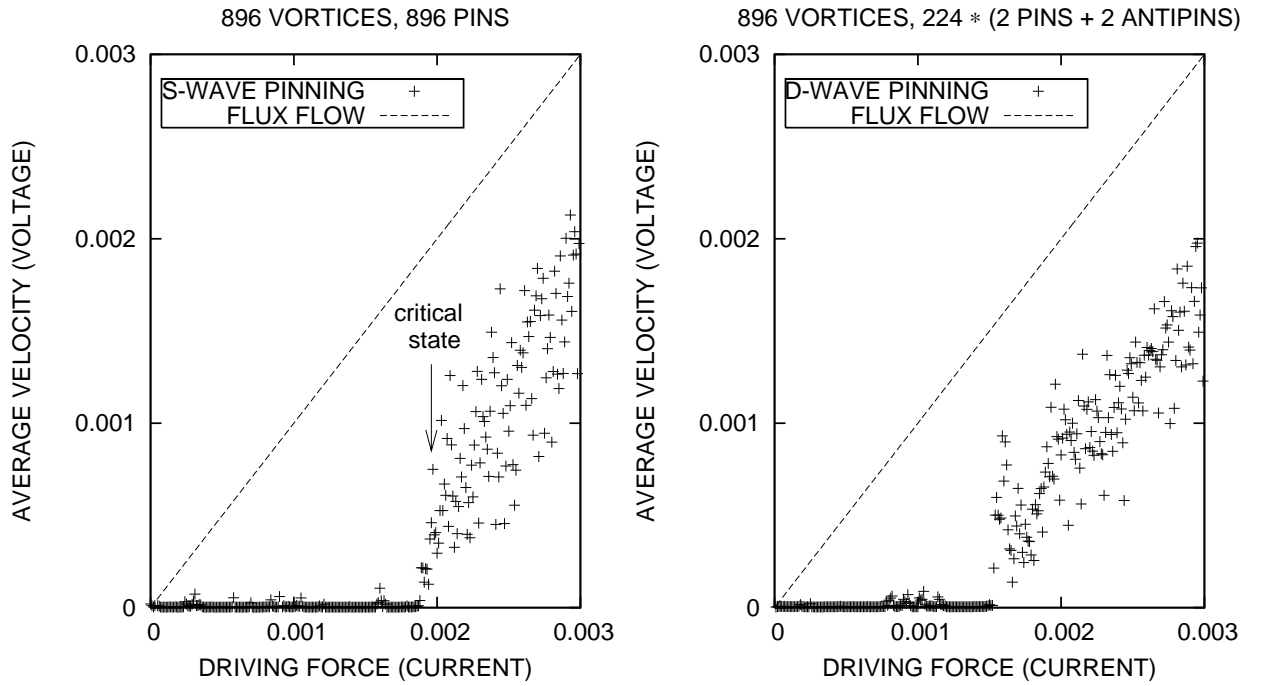


Figure 6: The left panel above shows the current-voltage curve obtained from driving 896 rigid vortex lines in the presence of an equal number of conventional (S-wave) columnar pins via the Langevin equation (8). All forces and velocities are given in units of $2\varepsilon_0 d/a_v$ and of $2\varepsilon_0 d/\eta a_v$, respectively. The right panel above depicts the current voltage curve obtained from driving 896 rigid vortex lines in the presence of 224 quadrupolar columnar pins. Each component pin/antipin line has a strength and range equal to that of the conventional S-wave columnar pins. (See fig. 3.)